Proton drip-line nuclei in relativistic Hartree-Bogoliubov theory

Vretenar, Dario; Lalazissis, G. A.; Ring, Peter

Source / Izvornik: **Physical Review C - Nuclear Physics, 1998, 57, 3071 - 3078**

Journal article, Published version
Rad u časopisu, Objavljena verzija rada (izdavačev PDF)

https://doi.org/10.1103/PhysRevC.57.3071

Permanent link / Trajna poveznica: https://urn.nsk.hr/urn:nbn:hr:217:925932

Proton drip-line nuclei in relativistic Hartree-Bogoliubov theory

D. Vretenar,[1] G. A. Lalazissis,[2] and P. Ring[2]
[1]*Physics Department, Faculty of Science, University of Zagreb, Croatia*
[2]*Physik-Department der Technischen Universität München, Garching, Germany*
(Received 22 December 1997)

Ground-state properties of spherical even-even nuclei $14 \leqslant Z \leqslant 28$ and $N = 18,20,22$ are described in the framework of relativistic Hartree-Bogoliubov (RHB) theory. The model uses the NL3 effective interaction in the mean-field Lagrangian, and describes pairing correlations by the pairing part of the finite range Gogny interaction D1S. Binding energies, two-proton separation energies, and proton rms radii that result from fully self-consistent RHB solutions are compared with experimental data. The model predicts the location of the proton drip line. The isospin dependence of the effective spin-orbit potential is discussed, as well as pairing properties that result from the finite range interaction in the pp channel. [S0556-2813(98)05906-8]

PACS number(s): 21.10.Dr, 21.10.Ft, 21.60.Jz, 27.30.+t

I. RELATIVISTIC HARTREE-BOGOLIUBOV THEORY WITH FINITE RANGE PAIRING INTERACTION

The structure of proton-rich nuclei presents many interesting phenomena which are very important both for nuclear physics and astrophysics. These nuclei are characterized by exotic ground-state decay properties such as direct emission of charged particles and β decays with large Q values. The properties of most proton-rich nuclei should also play an important role in the process of nucleosynthesis by rapid-proton capture. In addition to decay properties (particle emission, β decay), of fundamental importance are studies of atomic masses and separation energies, and especially the precise location of proton drip lines. On the other hand, nuclear-structure models can be compared in detailed theoretical studies of nuclei with a large proton excess. In particular, for proton-rich nuclei in the $sd-f$ shell ($10 \leqslant Z \leqslant 28$) predictions of the nuclear shell model can be compared with results of models that are based on the mean-field approach. Shell-model calculations of proton-rich nuclei with $37 \leqslant A \leqslant 48$ have recently been reported in Ref. [1], and the structure of proton-drip line around ^{48}Ni has been investigated in the framework of the self-consistent mean-field theory in Ref. [2]. In addition to nonrelativistic Hartree-Fock and Hartree-Fock-Bogoliubov models, in Ref. [2] also the relativistic mean-field model has been used, with pairing properties described in the BCS approximation. While this approximation is acceptable for nuclei close to the β-stability line, as we move away from the valley of β-stable nuclei the ground-state properties calculated with the BCS scheme become unreliable. For proton-rich nuclei this problem might be less critical than for nuclei at the neutron drip line, but nevertheless we expect a much better description of ground-state properties in a framework which provides a unified description of mean-field and pairing correlations.

In the present study we report the application of relativistic Hartree-Bogoliubov (RHB) theory to the structure of proton-rich nuclei. Models based on quantum hadrodynamics have been extensively applied in calculations of nuclear matter and properties of finite nuclei throughout the periodic table. In the self-consistent mean-field approximation, detailed calculations have been performed for a variety of nuclear structure phenomena [3]. For open shell nuclei pairing correlations have been included in the usual BCS approximation scheme, but also more consistently in the Hartree-Bogoliubov framework. RHB presents a relativistic extension of the Hartree-Fock-Bogoliubov (HFB) theory. It was derived in Ref. [4] in an attempt to develop a unified framework in which relativistic mean-field and pairing correlations could be described simultaneously. As in ordinary HFB, the ground state of a nucleus $|\Phi\rangle$ is described as a vacuum with respect to independent quasiparticle operators, which are defined by a unitary Bogoliubov transformation of the single-nucleon creation and annihilation operators. The generalized single-nucleon Hamiltonian contains two average potentials: the self-consistent mean-field $\hat{\Gamma}$ which encloses all the long-range ph correlations, and a pairing field $\hat{\Delta}$ which sums up the pp correlations. The expectation value of the nuclear Hamiltonian (nonrelativistic or Dirac) $\langle\Phi|\hat{H}|\Phi\rangle$ is a function of the Hermitian density matrix ρ, and the antisymmetric pairing tensor κ. The variation of the energy functional with respect to ρ and κ produces the single quasiparticle Hartree-Fock-Bogoliubov equations [5] in the nonrelativistic framework. In the relativistic extension [4] the Hartree approximation is employed for the self-consistent mean field, and the resulting relativistic Hartree-Bogoliubov (RHB) equations read

$$\begin{pmatrix} \hat{h}_D - m - \lambda & \hat{\Delta} \\ -\hat{\Delta}^* & -\hat{h}_D + m + \lambda \end{pmatrix} \begin{pmatrix} U(\mathbf{r}) \\ V(\mathbf{r}) \end{pmatrix} = E_k \begin{pmatrix} U(\mathbf{r}) \\ V(\mathbf{r}) \end{pmatrix}, \quad (1)$$

where $\hat{h}_D$ is the single-nucleon Dirac Hamiltonian (2) and m is the nucleon mass. The chemical potential λ has to be determined by the particle number subsidiary condition, in order that the expectation value of the particle number operator in the ground state equals the number of nucleons. The column vectors denote the quasiparticle wave functions, and E_k are the quasiparticle energies. The Dirac Hamiltonian

$$\hat{h}_D = -i\boldsymbol{\alpha}\cdot\nabla + \beta(m+g_\sigma\sigma) + g_\omega\omega^0 + g_\rho\tau_3\rho_3^0 + e\frac{(1-\tau_3)}{2}A^0 \tag{2}$$

contains the mean-field potentials of the isoscalar scalar σ meson, the isoscalar vector ω meson, and the isovector vector ρ meson. A^0 is the electrostatic potential. The RHB equations have to be solved self-consistently, with potentials determined in the mean-field approximation from solutions of Klein-Gordon equations

$$[-\Delta + m_\sigma^2]\sigma(\mathbf{r}) = -g_\sigma\rho_s(\mathbf{r}) - g_2\sigma^2(\mathbf{r}) - g_3\sigma^3(\mathbf{r}), \tag{3}$$

$$[-\Delta + m_\omega^2]\omega^0(\mathbf{r}) = -g_\omega\rho_v(\mathbf{r}), \tag{4}$$

$$[-\Delta + m_\rho^2]\rho^0(\mathbf{r}) = -g_\rho\rho_3(\mathbf{r}), \tag{5}$$

$$-\Delta A^0(\mathbf{r}) = e\rho_p(\mathbf{r}), \tag{6}$$

for the σ meson, ω meson, ρ meson, and photon field, respectively. The spatial components $\boldsymbol{\omega}$, ρ_3, and $\mathbf{A}$ vanish due to time-reversal symmetry. The equation for the σ meson contains the nonlinear σ self-interaction terms [6]. Because of charge conservation, only the three-component of the isovector ρ meson contributes. The source terms in Eqs. (3)–(6) are sums of bilinear products of baryon amplitudes

$$\rho_s(\mathbf{r}) = \sum_{E_k>0} V_k^\dagger(\mathbf{r})\gamma^0 V_k(\mathbf{r}), \tag{7}$$

$$\rho_v(\mathbf{r}) = \sum_{E_k>0} V_k^\dagger(\mathbf{r}) V_k(\mathbf{r}), \tag{8}$$

$$\rho_3(\mathbf{r}) = \sum_{E_k>0} V_k^\dagger(\mathbf{r})\tau_3 V_k(\mathbf{r}), \tag{9}$$

$$\rho_{\rm em}(\mathbf{r}) = \sum_{E_k>0} V_k^\dagger(\mathbf{r})\frac{1-\tau_3}{2} V_k(\mathbf{r}), \tag{10}$$

where the sums run over all positive energy states. The pairing field $\hat{\Delta}$ in Eq. (1) is defined

$$\Delta_{ab}(\mathbf{r},\mathbf{r}') = \frac{1}{2}\sum_{c,d} V_{abcd}(\mathbf{r},\mathbf{r}')\boldsymbol{\kappa}_{cd}(\mathbf{r},\mathbf{r}'), \tag{11}$$

where a,b,c,d denote quantum numbers that specify the single-nucleon states. $V_{abcd}(\mathbf{r},\mathbf{r}')$ are matrix elements of a general two-body pairing interaction, and the pairing tensor is defined

$$\boldsymbol{\kappa}_{cd}(\mathbf{r},\mathbf{r}') = \sum_{E_k>0} U_{ck}^*(\mathbf{r})V_{dk}(\mathbf{r}'). \tag{12}$$

Of course we only consider contributions from $J=0$ pairs to the pairing matrix elements, and therefore $c=d$ for the quantum numbers of single-nucleon states in the expression for the pairing tensor. The second index k denotes the kth eigenvector with the spherical quantum numbers c, and the sum is over eigenvectors with positive energy.

In the relativistic Hartree-Bogoliubov theory pairing correlations result from the one-meson exchange (σ, ω, and ρ mesons) [4]. However, if for the pairing part of the interaction one uses the coupling constants from standard parameter sets of the relativistic mean-field model, the resulting pairing correlations are much too strong. The repulsion produced by the exchange of vector mesons at short distances results in a pairing gap at the Fermi surface that is by a factor of 3 too large. This is not surprising, since in general the effective interactions in the particle-hole and particle-particle channels do not have to be identical. In a first-order approximation, the effective interaction contained in the mean field $\hat{\Gamma}$ is a G matrix, the sum over all ladder diagrams. The effective force in the pp channel, i.e., in the pairing potential $\hat{\Delta}$, should be the K matrix, the sum of all diagrams irreducible in pp direction. However, very little is known about this matrix in the relativistic framework. And although the relativistic theory of pairing presents a very active area of research [7,8], only phenomenological effective forces have been shown to produce reliable results when applied to finite nuclei, especially in exotic regions. In the present work we employ a two-body finite-range interaction of the Gogny type [9] in the pp channel of RHB:

$$V^{pp}(1,2) = \sum_{i=1,2} e^{-[(\mathbf{r}_1-\mathbf{r}_2)/\mu_i]^2} \times (W_i + B_i P^\sigma - H_i P^\tau - M_i P^\sigma P^\tau), \tag{13}$$

with the parameters μ_i, W_i, B_i, H_i, and M_i ($i=1,2$). The pairing interaction is a sum of two Gaussians with finite range and properly chosen spin and isospin dependence. The Gogny force has been very carefully adjusted to reproduce selected global properties of spherical nuclei and of nuclear matter. In the pairing channel its basic advantage is the finite range, which automatically guarantees a proper cutoff in momentum space. This interaction was employed in the RHB calculations of Ref. [10]. For the D1S [9] parameter set of the interaction in the pairing channel, the model was applied in the study of several isotope chains of spherical Pb, Sn, and Zr nuclei. In Refs. [11–13] we have used RHB in coordinate space with the D1S Gogny interaction to describe properties of light nuclear systems (C, N, O, F, Ne, Na, Mg) with large neutron excess, as well as ground states of Ni ($28\leqslant N\leqslant 50$) and Sn ($50\leqslant N\leqslant 82$) isotopes.

The eigensolutions of Eq. (1) form a set of orthogonal and normalized single quasiparticle states. The corresponding eigenvalues are the single quasiparticle energies. The self-consistent iteration procedure is performed in the basis of quasiparticle states. The resulting quasiparticle eigenspectrum is then transformed into the canonical basis of single-particle states, in which the RHB ground state takes the BCS form. The transformation determines the energies and occupation probabilities of the canonical states.

For nuclear systems with spherical symmetry the fields $\sigma(r)$, $\omega^0(r)$, $\rho^0(r)$, and $A^0(r)$ depend only on the radial coordinate r. The nucleon spinors U_k (V_k) in Eq. (1) are characterized by the angular momentum j, its z projection m, parity π, and the isospin $t_3=\pm\frac{1}{2}$ for the neutron and proton. The two Dirac spinors $U_k(\mathbf{r})$ and $V_k(\mathbf{r})$ are defined

$$U_k(V_k)(\mathbf{r},s,t_3)=\begin{pmatrix} g_{U(V)}(r)\Omega_{j,l,m}(\theta,\varphi,s) \\ if_{U(V)}(r)\Omega_{j,\tilde{l},m}(\theta,\varphi,s)\end{pmatrix}\chi_\tau(t_3). \tag{14}$$

$g(r)$ and $f(r)$ are radial amplitudes, χ_τ is the isospin function, and Ω_{jlm} is the tensor product of the orbital and spin functions

$$\Omega_{j,l,m}(\theta,\varphi,s)=\sum_{m_s,m_l}\left\langle \frac{1}{2}m_s l m_l \middle| jm\right\rangle \chi^{\frac{1}{2}}_{m_s}Y_{lm_l}(\theta,\varphi). \tag{15}$$

The two-component functions

$$\Phi_U(r):=\begin{pmatrix} g_U(r) \\ if_U(r)\end{pmatrix} \quad \text{and} \quad \Phi_V(r):=\begin{pmatrix} g_V(r) \\ if_V(r)\end{pmatrix}, \tag{16}$$

are solutions of the Dirac-Hartree-Bogoliubov equations

$$\begin{aligned}[\hat{h}_D(r)-m-\lambda]\Phi_U(r)+\int_0^\infty dr' r'^2\Delta(r,r')\Phi_V(r') \\ =E\Phi_U(r), \\ [-\hat{h}_D(r)+m+\lambda]\Phi_V(r)+\int_0^\infty dr' r'^2\Delta(r,r')\Phi_U(r') \\ =E\Phi_V(r).\end{aligned} \tag{17}$$

The self-consistent solution of the Dirac-Hartree-Bogoliubov integrodifferential eigenvalue equations and Klein-Gordon equations for the meson fields determines the nuclear ground state. In Refs. [11,12,14,15] we have used finite element methods in the coordinate space discretization of the coupled system of equations. Coordinate space solutions of the RHB equations are essential for a correct description of nuclear structure phenomena that originate from large spatial extensions of nucleon densities. These include, for example, neutron skins and halos in very neutron-rich nuclei. In less exotic nuclei on the neutron-rich side, or for proton-rich nuclei, an expansion in a large oscillator basis should provide sufficiently accurate solutions [16,17]. In particular, proton-rich nuclei are stabilized by the Coulomb barrier which tends to localize the proton density in the nuclear interior and thus prevents the formation of objects with extreme spatial extension. In the present work we employ the procedure of Refs. [10,13], and solve the Dirac-Hartree-Bogoliubov equations and the equations for the meson fields by expanding the nucleon spinors $U_k(\mathbf{r})$ and $V_k(\mathbf{r})$, and the meson fields in a basis of spherical harmonic oscillators for $N=20$ oscillator shells [18]. However, in order to verify that our final conclusions do not depend on the method of solution, for nuclei at the proton drip line we have also performed RHB calculations in coordinate space [15]. In particular, coordinate space solutions have confirmed our predictions for the location of the proton drip line.

II. GROUND-STATE PROPERTIES OF PROTON-RICH NUCLEI

In the present application of the relativistic Hartree-Bogoliubov theory we describe the ground-state properties of spherical even-even nuclei $14\leqslant Z\leqslant 28$ and $N=18,20,22$. While for these neutron numbers the nuclei with $14\leqslant Z\leqslant 20$ are not really very proton rich, nevertheless they will be useful for a comparison of the model calculations with experimental data. We are particularly interested in the predictions of the model for the proton-rich nuclei in the $1f_{7/2}$ region. These nuclei have recently been extensively investigated in experiments involving fragmentation of ^{58}Ni [19–22]. The principal motivation of many experimental studies in this region is the possible occurrence of the two-proton ground-state radioactivity. In particular, the region around ^{48}Ni is expected to contain nuclei which are two-proton emitters. On the other hand, because of the Coulomb barrier at the proton drip line, the emission of a pair of protons may be strongly delayed for nuclei with small negative two-proton separation energies.

The input for our calculations are the coupling constants and masses for the effective mean-field Lagrangian, and the effective interaction in the pairing channel. In the analysis of light neutron-rich nuclei in Refs. [11,12,14], as well as in the study of ground-state properties of Ni and Sn isotopes [13], we have used the NL3 parameter set for the effective mean-field Lagrangian in the ph channel. The effective interaction NL3 has been derived [23] by adjusting model calculations to bulk properties of a large number of spherical nuclei. Properties calculated with the NL3 effective interaction are found to be in very good agreement with experimental data for nuclei at and away from the line of β stability. In Ref. [24] it has been shown that constrained relativistic mean-field (RMF) calculations with the NL3 effective force reproduce the excitation energies of superdeformed minima relative to the ground state in ^{194}Hg and ^{194}Pb. In the same work the NL3 interaction was also used for calculations of binding energies and deformation parameters of rare-earth nuclei. In the present study we employ the NL3 effective force on the proton-rich side of the β-stability line. In view of the fact that all the results obtained so far indicate that NL3 is probably the best effective RMF interaction, the main purpose of the analysis is to study how well the properties predicted by the NL3 force compare with experimental data for proton-rich nuclei. However, in order to be more specific in our predictions for the exact location of the proton drip line, we will also use two additional standard RMF effective interactions: NL1 [25] and NL-SH [26]. These effective forces have been used in many analyses to calculate properties of nuclear matter and of finite nuclei, and generally produce very good results for nuclei close to the β-stability line. In particular, the effective interaction NL1 was also used in the RHB +Gogny calculations of Ref. [10]

In most applications of relativistic mean-field theory pairing correlations have been included in the form of a simple BCS approximation, with a monopole pairing force adjusted to the experimental odd-even mass differences [18]. For nuclei far from the valley of β stability this approach becomes unreliable, especially in the calculation of properties that crucially depend on the spatial extensions of nucleon densities. The BCS description of the scattering of nucleonic pairs from bound states to the positive energy particle continuum produces an unphysical component in the nucleon density with the wrong asymptotic behavior [16,17]. This effect is more pronounced for neutron-rich nuclei, for which the cou-

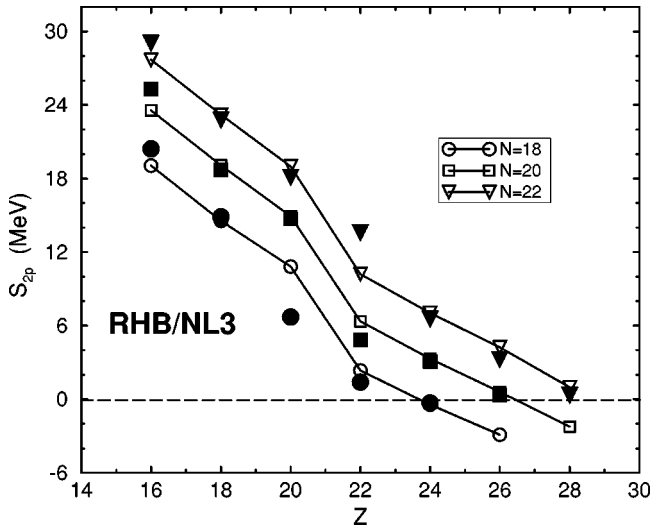

FIG. 1. Comparison between RHB/NL3 and experimental two-proton separation energies for $N=18,20,22$ isotones. Black symbols denote empirical values; lines connect symbols which correspond to calculated values.

pling to the particle continuum is particularly important. For proton-rich nuclei the Coulomb barrier confines the protons in the interior of the nucleus, and therefore the effect of the coupling to the continuum is weaker. However, if pairing correlations are described in the unified framework of the RHB scheme (or HFB in the nonrelativistic approach), the nucleon densities display a correct asymptotic behavior. The effective interactions that have been used in the pairing channel of RHB are the pairing part of the Gogny force and the density-dependent δ force. The finite-range interaction provides an automatic cutoff of high momentum components, while an artificial energy cutoff has to be included in the calculation with zero-range forces. On the other hand, the density-dependent interaction can be adjusted to produce surface peaked pairing fields, which can be important for a correct description of spatial distribution of densities. A fully self-consistent RHB model in coordinate space, with a density-dependent interaction of zero-range (δ force), has been used to describe the two-neutron halo in ^{11}Li [27]. In the present study we employ the pairing part of the Gogny interaction in the pp channel, with the parameter set D1S [9].

In Fig. 1 we display the two-proton separation energies

$$S_{2p}(Z,N)=B_p(Z,N)-B_p(Z-2,N) \tag{18}$$

for the even-even nuclei $14\leqslant Z\leqslant 28$ and $N=18,20,22$. The values that correspond to the self-consistent RHB ground states are compared with experimental data and extrapolated values from Ref. [28]. We notice that the theoretical values reproduce in detail the experimental separation energies, except for ^{38}Ca and ^{44}Ti. In order to understand better this result, in Table I we compare the calculated total binding energies for the $N=18,20,22$ isotones with empirical values. We find that our model results are in very good agreement with experimental data when one of the shells (proton or neutron) is closed, or when valence protons and neutrons occupy different major shells (i.e., below and above N and/or $Z=20$). The absolute differences between the calculated and experimental masses are less than 2 MeV. The differences are larger when both proton and neutron valence particles (holes) occupy the same major shell, and especially for the $N=Z$ nuclei ^{36}Ar and ^{44}Ti. This seems to be a clear indication that for these nuclei additional correlations should be taken into account. In particular, proton-neutron pairing could have a strong influence on the masses. Proton-neutron short-range correlations are not included in our model.

The results should be also compared with recently reported self-consistent mean-field calculations of Ref. [2], and with properties of proton-rich nuclei calculated within the framework of the nuclear shell model [1]. The calculations of Ref. [2] have been performed for several mean-field models (Hartree-Fock, Hartree-Fock-Bogoliubov, and relativistic mean-field), and for a number of effective interactions. The results systematically predict the two-proton drip line to lie between ^{42}Cr and ^{44}Cr, ^{44}Fe and ^{46}Fe, and ^{48}Ni and ^{50}Ni. Very recent studies of proton drip-line nuclei in this region have been performed in experiments based on ^{58}Ni fragmentation on a beryllium target [21,22]. In Ref. [21] in particular, evidence has been reported for particle stability of ^{50}Ni. In the shell-model calculations of Ref. [1] absolute binding energies were evaluated by computing the Coulomb energy shifts between mirror nuclei, and adding this shift to the experimentally determined binding energy of the neutron-rich isotope. The calculated two-proton separation energies predicted a proton drip line in agreement with experimental data and with the mean-field results [2]. Compared to the results of the present study, the shell-model total binding energies are in somewhat better agreement with experimental data. However, the two models give almost identical values for the extracted two-proton separation energies of the drip-line nuclei. The self-consistent RHB NL3+D1S two-proton separation energies at the drip line are also very close to the values that result from nonrelativistic HFB+Gogny (D1S) calculation of Ref. [2].

TABLE I. Comparison between calculated and empirical binding energies. All values are in units of MeV; empirical values are displayed in parentheses.

^{32}Si	269.02 (271.41)	^{40}Ar	343.97 (343.81)	^{44}Cr	351.65 (349.99)
^{34}Si	284.42 (283.43)	^{38}Ca	313.11 (313.04)	^{46}Cr	380.19 (381.98)
^{36}Si	293.08 (292.02)	^{40}Ca	341.99 (342.05)	^{44}Fe	312.07 (-)
^{34}S	288.10 (291.84)	^{42}Ca	362.95 (361.90)	^{46}Fe	352.25 (350.20)
^{36}S	307.98 (308.71)	^{40}Ti	315.39 (314.49)	^{48}Fe	384.42 (385.19)
^{38}S	320.77 (321.05)	^{42}Ti	348.35 (346.91)	^{46}Ni	306.72 (-)
^{36}Ar	302.52 (306.71)	^{44}Ti	373.15 (375.47)	^{48}Ni	349.92 (-)
^{38}Ar	327.34 (327.06)	^{42}Cr	314.94 (314.20)	^{50}Ni	385.52 (385.50)

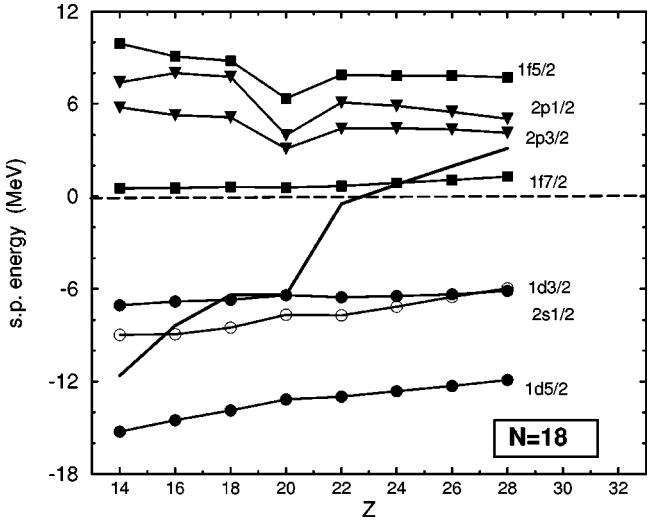

FIG. 2. The proton single-particle levels for the $N=18$ isotones. Solid lines denote the neutron Fermi level. The energies in the canonical basis correspond to ground-state solutions calculated with the NL3 effective force of the mean-field Lagrangian. The parameter set D1S is used for the finite-range Gogny-type interaction in the pairing channel.

By using a fully microscopic and self-consistent model for the calculation of binding energies, we have the possibility to analyze in detail the single-proton levels. In Figs. 2, 3, and 4 we display the proton single-particle energies in the canonical basis as functions of proton number for the $N=18,20,22$ isotones, respectively. The thick solid lines denote the corresponding Fermi levels. The proton energies are not single-particle energies (i.e., the eigenvalues of the *p-h* Hamiltonian h_D) but the diagonal matrix elements of h_D in the canonical basis. Therefore the phase space that corresponds to positive-energy states should not be confused with the continuum of scattering states which asymptotically behave as plane waves. The RHB ground-state wave function can be written either in the quasiparticle basis as a product of independent quasiparticle states, or in the *canonical basis* as a highly correlated BCS state. In the *canonical basis* nucleons occupy single-particle states. The canonical states are

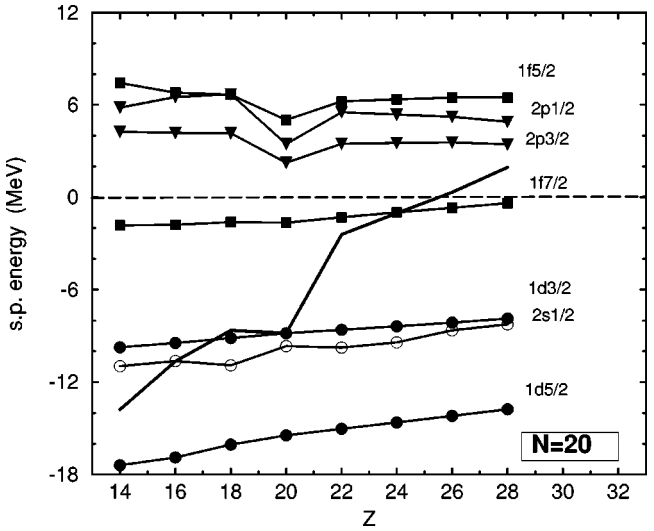

FIG. 3. Same as in Fig. 2, but for the $N=20$ isotones.

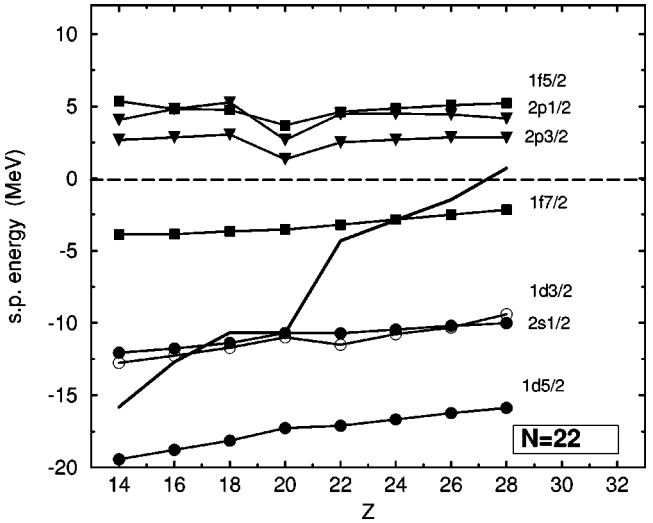

FIG. 4. Same as in Fig. 2, but for the $N=22$ isotones.

eigenstates of the RHB density matrix. The eigenvalues are the corresponding occupation numbers. Since the density matrices in RHB are always localized, all canonical-basis single-particle wave functions vanish at large distances.

Although the proton levels do not change much with Z, we observe a consistent decrease in the energy splitting between the spin-orbit partners $1d_{5/2}$-$1d_{3/2}$ and $2p_{3/2}$-$2p_{1/2}$ with increasing proton number. We will show that this decrease results from the reduction of the spin-orbit term of the effective potential [14]. The $1f_{7/2}$ orbital is unbound for all $N=18$ isotones, and is very slightly bound for $N=20$. The Fermi level displays a sharp increase with Z for all three isotone chains. In principle, a positive value of λ should indicate which nuclei are beyond the proton drip line, i.e., which nuclei are ground-state proton emitters. In particular, for ^{42}Cr, ^{46}Fe, and ^{50}Ni we find $\lambda>0$. This is somewhat surprising, since for ^{46}Fe and ^{50}Ni the calculated two-proton separation energies are positive. We have performed RHB calculations with the effective interactions NL1 and NLSH, but also for these forces the Fermi level is positive for ^{42}Cr, ^{46}Fe, and ^{50}Ni. For these three nuclei we have also verified the results by performing coordinate space RHB calculations. The results are practically identical to those obtained with the oscillator expansion method; the Fermi levels for these three nuclei have positive values. Therefore it appears that there are cases at the drip line for which the definition of the two-particle separation energy (18) does not correspond to the physical interpretation of the chemical potential.

In Fig. 5 we show the self-consistent ground-state proton densities for the $N=20$ isotones. The density profiles display shell effects in the bulk and a gradual increase of proton radii. In the inset of Fig. 5 we include the corresponding values for the surface thickness and diffuseness parameter. The surface thickness s is defined to be the change in radius required to reduce $\rho(r)/\rho_0$ from 0.9 to 0.1 (ρ_0 is the maximal value of the neutron density; because of shell effects we could not use for ρ_0 the density in the center of the nucleus). The diffuseness parameter α is determined by fitting the neutron density profiles to the Fermi distribution

$$\rho(r)=\rho_0\left[1+\exp\left(\frac{r-R_0}{\alpha}\right)\right]^{-1}, \tag{19}$$

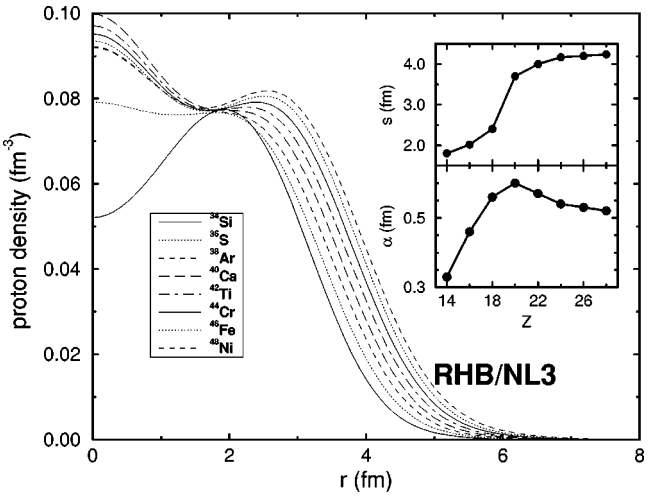

FIG. 5. Self-consistent RHB single-proton density distributions for the $N=20$ isotones, calculated with the NL3 effective interaction.

where R_0 is the half-density radius. In going away from the valley of β-stable nuclei, generally the proton surface thickness increases and the surface becomes more diffuse. However, while s increases from Si to Ni, the diffuseness parameter α has a maximum at $Z=20$. It appears that, as protons fill the $1f_{7/2}$ orbital, the proton surface becomes slightly less diffuse. This could be due to the stronger influence of the Coulomb barrier. In Fig. 6 we display the self-consistent proton potentials for the $N=20$ isotones, and in the inset the details of the potentials in the region of the Coulomb barrier. We notice how the Coulomb barrier increases from 3 MeV for ^{34}Si, to 6 MeV in ^{48}Ni. We include also ^{48}Ni in our figures for the $N=20$ isotones, although this nucleus is not particle stable in our calculations.

In Fig. 7 we display the proton rms radii for $N=18,20,22$ isotones, respectively. The calculated values are compared with experimental data for proton radii from Ref. [29]. Except for ^{32}Si, we find an excellent agreement between experimental data and values calculated with the NL3 effective force with the D1S Gogny interaction in the pairing

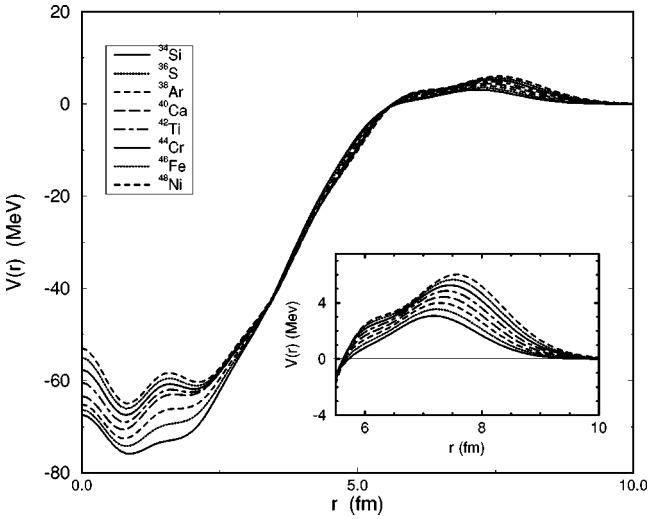

FIG. 6. Self-consistent proton potentials for the $N=20$ isotones. In the inset the details of the Coulomb barriers are shown.

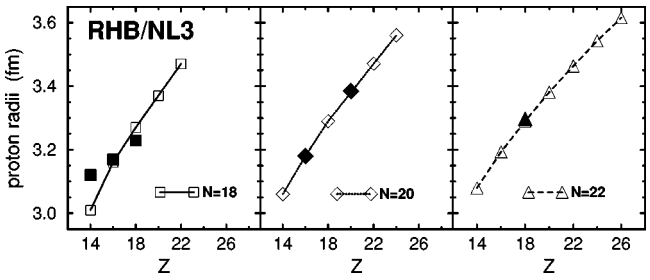

FIG. 7. Calculated proton rms radii for $N=18,20,22$ isotones compared with experimental data.

channel. The model predicts a uniform increase of rms radii with the number of protons.

In an analysis of ground-state properties of light neutron-rich nuclei [14], we have shown that the relativistic mean-field model predicts a strong isospin dependence of the effective spin-orbit potential. With the increase of the number of neutrons the effective spin-orbit interaction becomes weaker and the magnitude of the spin-orbit term in the single nucleon potential is significantly reduced. This results in a reduction of the energy splittings for spin-orbit partners. The reduction in the surface region was found to be as large as $\approx 40\%$ for Ne isotopes at the drip line. In Ref. [13] similar results were found for the Ni and Sn isotopes. The spin-orbit potential originates from the addition of two large fields: the field of the vector mesons (short-range repulsion), and the scalar field of the σ meson (intermediate attraction). In the first-order approximation, and assuming spherical symmetry, the spin-orbit term can be written as

$$V_{\rm so}=\frac{1}{r}\frac{\partial}{\partial r}V_{ls}(r), \tag{20}$$

where V_{ls} is the spin-orbit potential [30]

$$V_{ls}=\frac{m}{m_{\rm eff}}(V-S). \tag{21}$$

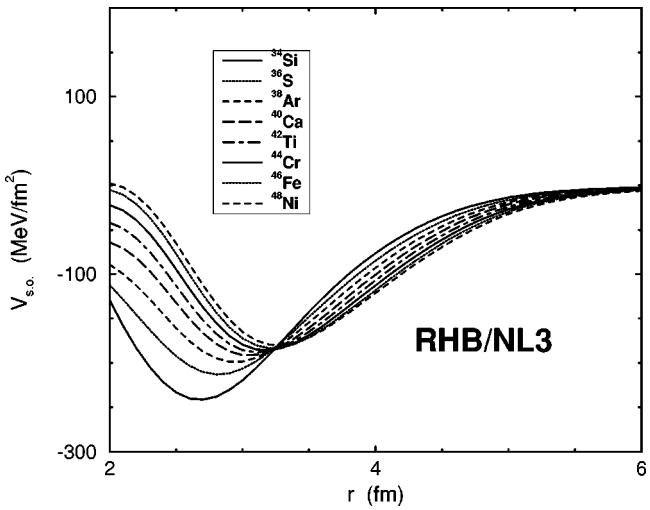

FIG. 8. Radial dependence of the spin-orbit term of the proton potential in self-consistent solutions for ground-states of the $N=20$ isotones.

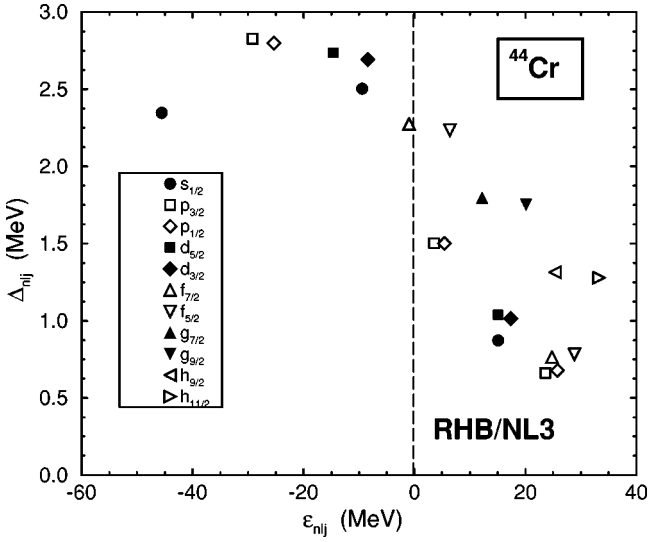

FIG. 9. Average values of the proton canonical pairing gaps as functions of canonical single-particle energies for states that correspond to the self-consistent ground state of ^{44}Cr. The NL3 parametrization has been used for the mean-field Lagrangian, and the parameter set D1S for the pairing interaction.

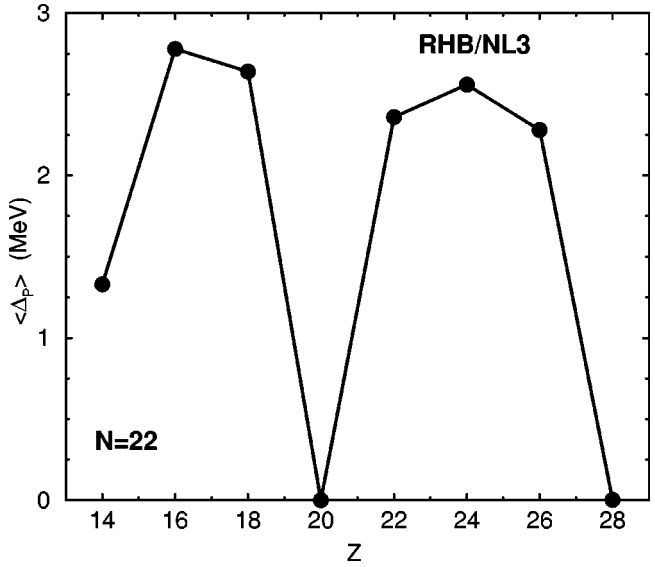

FIG. 10. Average proton pairing gaps $\langle\Delta_p\rangle$ of the $N=22$ isotones.

V and S denote the repulsive vector and the attractive scalar potentials, respectively [see the Dirac Hamiltonian (2)]. $m_{\rm eff}$ is the effective mass

$$m_{\rm eff}=m-\frac{1}{2}(V-S). \tag{22}$$

Using the vector and scalar potentials from the NL3 self-consistent ground-state solutions, we have computed from Eqs. (20)–(22) the spin-orbit terms of the effective proton potentials for the $N=20$ isotones. They are shown in Fig. 8 as function of the radial distance from the center of the nucleus. The magnitude of the spin-orbit term $V_{\rm so}$ decreases as we add more protons, i.e., as we move away from β-stable nuclei. From ^{34}Si to ^{48}Ni, the reduction is $\approx$20% in the surface region. The minimum of $V_{\rm so}$ is also shifted outwards, and this reflects the larger spatial extension of the proton densities. However, we note that the reduction of $V_{\rm so}$ for protons is considerably smaller than the one calculated for neutrons in Refs. [14,13] ($\approx 35-40$ %).

The properties of the finite-range and density-independent pairing interaction are illustrated in Figs. 9 and 10. In Fig. 9 we plot the average values of the proton canonical pairing gaps Δ_{nlj} as functions of canonical single-particle energies. The gaps are displayed for canonical states that correspond to the self-consistent ground state of ^{44}Cr. Δ_{nlj} are the diagonal matrix elements of the pairing part of the RHB single-nucleon Hamiltonian in the canonical basis. Although not completely equivalent, Δ_{nlj} corresponds to the pairing gap in BCS theory. A very detailed discussion of HFB equations in the canonical basis can be found in Ref. [17]. The pairing gaps have relatively large values for deep-hole states. This is related to the volume character of the Gogny interaction in the pairing channel. The average value at the Fermi surface is between 1.5 and 2 MeV, and Δ_{nlj} slowly decrease for canonical states in the single-proton continuum. In Fig. 10 we display the averages of the proton pairing gaps for occupied canonical states

$$\langle\Delta_p\rangle=\frac{\sum_{nlj}\Delta_{nlj}v^2_{nlj}}{\sum_{nlj}v^2_{nlj}}, \tag{23}$$

where v^2_{nlj} are the occupation probabilities. The values of $\langle\Delta_p\rangle$ for the $N=22$ isotones are plotted as function of the proton number. The average proton gap increases to almost 3 MeV for ^{38}Ar, then the pairing correlations disappear at shell closure $Z=20$. For the $1f_{7/2}$ orbital the value of $\langle\Delta_p\rangle$ is ≈ 2.5 MeV.

In conclusion, this study presents the first application of the relativistic Hartree-Bogoliubov theory to the description of ground-state properties of proton-rich nuclei. A detailed analysis of spherical even-even nuclei with $14\leqslant Z\leqslant 28$ and $N=18,20,22$ has been performed. The NL3 parameter set has been used for the effective mean-field Lagrangian in the ph channel, and pairing correlations have been described by the finite-range Gogny interaction D1S. In a comparison with available experimental data it has been shown that the NL3 + Gogny D1S effective interaction provides a very good description of binding energies, two-proton separation energies and proton rms radii. Model predictions for the proton drip line agree with recently reported calculations in the framework of the nuclear shell model and with results of nonrelativistic HF and HFB studies. For isotone chains we have also discussed the predicted reduction of the effective spin-orbit potential with the increase of the number of protons, as well as the resulting energy splittings between spin-orbit partners and modifications of surface properties.

[1] W. E. Ormand, Phys. Rev. C **53**, 214 (1996).
[2] W. Nazarewicz, J. Dobaczewski, T. R. Werner, J. A. Maruhn, P.-G. Reinhard, K. Rutz, C. R. Chinn, A. S. Umar, and M. R. Strayer, Phys. Rev. C **53**, 740 (1996).
[3] P. Ring, Prog. Part. Nucl. Phys. **37**, 193 (1996).
[4] H. Kucharek and P. Ring, Z. Phys. A **339**, 23 (1991).
[5] P. Ring and P. Schuck, *The Nuclear Many-Body Problem* (Springer-Verlag, Heidelberg, 1980).
[6] J. Boguta and A. R. Bodmer, Nucl. Phys. **A292**, 413 (1977).
[7] F. B. Guimarães, B. V. Carlson, and T. Frederico, Phys. Rev. C **54**, 2385 (1996).
[8] F. Matera, G. Fabbri, and A. Dellafiore, Phys. Rev. C **56**, 228 (1997).
[9] J. F. Berger, M. Girod, and D. Gogny, Nucl. Phys. **A428**, 32 (1984).
[10] T. Gonzalez-Llarena, J. L. Egido, G. A. Lalazissis, and P. Ring, Phys. Lett. B **379**, 13 (1996).
[11] W. Pöschl, D. Vretenar, G. A. Lalazissis, and P. Ring, Phys. Rev. Lett. **79**, 3841 (1997).
[12] G. A. Lalazissis, D. Vretenar, W. Pöschl, and P. Ring, Nucl. Phys. **A632**, 363 (1998).
[13] G. A. Lalazissis, D. Vretenar, and P. Ring, Phys. Rev. C **57**, 2294 (1998).
[14] G. A. Lalazissis, D. Vretenar, W. Pöschl, and P. Ring, Phys. Lett. B (in press).
[15] W. Pöschl, D. Vretenar, and P. Ring, Comput. Phys. Commun. **103**, 217 (1997).
[16] J. Dobaczewski, H. Flocard, and J. Treiner, Nucl. Phys. **A422**, 103 (1984).
[17] J. Dobaczewski, W. Nazarewicz, T. R. Werner, J. F. Berger, C. R. Chinn, and J. Dechargé, Phys. Rev. C **53**, 2809 (1996).
[18] Y. K. Gambhir, P. Ring, and A. Thimet, Ann. Phys. (N.Y.) **511**, 129 (1990).
[19] C. Détraz *et al.*, Nucl. Phys. **A519**, 529 (1990).
[20] V. Borrel *et al.*, Z. Phys. A **344**, 135 (1992).
[21] B. Blank *et al.*, Phys. Rev. C **50**, 2398 (1994).
[22] B. Blank *et al.*, Phys. Rev. Lett. **77**, 2893 (1996).
[23] G. A. Lalazissis, J. König, and P. Ring, Phys. Rev. C **55**, 540 (1997).
[24] G. A. Lalazissis and P. Ring, Phys. Lett. B (in press).
[25] P. G. Reinhard, M. Rufa, J. Maruhn, W. Greiner, and J. Friedrich, Z. Phys. A **323**, 13 (1986).
[26] M. M. Sharma, M. A. Nagarajan, and P. Ring, Phys. Lett. B **312**, 377 (1993).
[27] J. Meng and P. Ring, Phys. Rev. Lett. **77**, 3963 (1996).
[28] G. Audi and A. H. Wapstra, Nucl. Phys. **A595**, 409 (1995).
[29] H. de Vries, C. W. de Jager, and C. de Vries, At. Data Nucl. Data Tables **36**, 495 (1987).
[30] W. Koepf and P. Ring, Z. Phys. A **339**, 81 (1991).